Resonant nano-antennas for light trapping in plasmonic solar cells

2011 J. Phys. D: Appl. Phys. 44 185101

(http://iopscience.iop.org/0022-3727/44/18/185101)

IOP PUBLISHING JOURNAL OF PHYSICS D: APPLIED PHYSICS

J. Phys. D: Appl. Phys. **44** (2011) 185101 (9pp) doi:10.1088/0022-3727/44/18/185101

Resonant nano-antennas for light trapping in plasmonic solar cells

S Mokkapati[1], F J Beck[1], R de Waele[2], A Polman[2] and K R Catchpole[1]

[1] Centre for Sustainable Energy Systems, College of Engineering and Computer Science, The Australian National University, Canberra, Australia–0200
[2] Center for Nanophotonics, FOM Institute AMOLF, Science Park 104, 1098 XG Amsterdam, The Netherlands

E-mail: sudha.mokkapati@anu.edu.au

Received 24 November 2010, in final form 6 March 2011
Published 15 April 2011
Online at stacks.iop.org/JPhysD/44/185101

Abstract
We investigate the influence of nanoparticle height on light trapping in thin-film solar cells covered with metal nanoparticles. We show that in taller nanoparticles the scattering cross-section is enhanced by resonant excitation of plasmonic standing waves. Tall nanoparticles have higher coupling efficiency when placed on the illuminated surface of the cell than on the rear of the cell due to their forward scattering nature. One of the major factors affecting the coupling efficiency of these particles is the phase shift of surface plasmon polaritons propagating along the nanoparticle due to reflection from the Ag/Si or Ag/air interface. The high scattering cross-sections of tall nanoparticles on the illuminated surface of the cell could be exploited for efficient light trapping by modifying the coupling efficiency of nanoparticles by engineering this phase shift. We demonstrate that the path length enhancement (with a nanoparticle of height 500 nm) at an incident wavelength of 700 nm can be increased from ∼6 to ∼16 by modifying the phase shift at the Ag/air interface by coating the surface of the nanoparticle with a layer of Si.

(Some figures in this article are in colour only in the electronic version)

1. Introduction and approach

There has been an increased interest, in recent years, in wavelength-scale light trapping techniques for application to thin solar cells. Light scattering by metal nanoparticles due to excitation of plasmons is a promising technique for trapping light inside the active volume of a solar cell [1–10]. Plasmonic nanoparticles have been shown to give substantial photocurrent enhancements on thick substrates and on thin waveguides. The highest increase in photocurrent reported so far is 33% and 19% using random silver nanoparticle arrays placed on the surface of Si-on-insulator and Si-wafer-based solar cells, respectively [3]. The properties of the nanoparticle array that need to be optimized to maximize their light trapping efficiency include the nanoparticle size and shape [5, 11], the thickness and refractive index of dielectric layers between the solar cell and the nanoparticle array [12–14], the fractional surface coverage and the arrangement of the nanoparticles (random arrays and/or periodic arrays). Studies so far have demonstrated that flattened particles like hemispheres or discs have highest near-field coupling of radiation into the substrate [11], and that the scattering cross-section of the nanoparticles and the efficiency of coupling scattered radiation into the substrate depend critically on the spacer layer thickness and refractive index [11, 14]. Both random arrays [2] and quasi-periodic arrays [4] have experimentally demonstrated significant increase in the absorption in the solar cell, and theoretical studies have been published on optimizing the random/periodic arrays of nanoparticles [15, 16]. Experiments demonstrate that for thin GaAs solar cells, tall, high aspect ratio Ag nanoparticles result in an enhanced light absorption in the substrate compared to short (smaller aspect ratio) particles [4]. However, there has been no systematic study on the effect of nanoparticle height on the light-trapping properties.

In this paper we present a numerical study on the optimization of nanoparticle height for light-trapping applications. We systematically study the effect of nanoparticle height variation on the scattering cross-section,

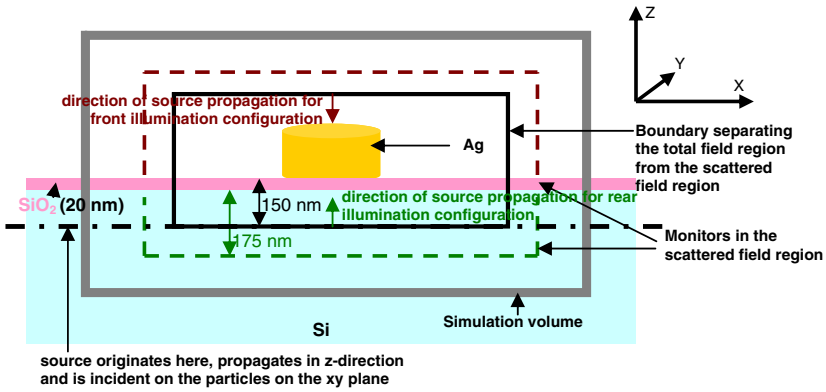

Figure 1. Schematic cross-section of the simulation set-up used for this study (not to scale). The nanoparticles studied are Ag cylinders (diameter 200 nm) with rounded off top and bottom surfaces (radius of curvature 20 nm) placed on Si with a 20 nm thick SiO_2 spacer layer. A TFSF source is incident on the particle from the air side or the substrate side and its origin is indicated for the rear illumination configuration using the black dashed–dotted line. The direction of source propagation is indicated by red arrow for front illumination configuration and by a green arrow for the rear illumination configuration. The volume bounded by solid black lines separates the total field region from the scattered field region. The fields detected/measured inside this volume are total field (incident + scattered), while outside this volume, the fields detected are only due to scattered light. The grey line indicates the simulation volume and the dashed lines (green and red) indicate the monitors used for calculating the scattering cross-sections of the particles and fraction of scattered power coupled into the substrate. The scattered fields are monitored at a depth of 175 nm from the substrate surface.

fraction of light scattered into the substrate and thus the ability to enhance the absorption inside a Si substrate. Results are presented for both front illumination (particles on the illuminated surface of the substrate) and rear illumination (particles on the rear of the substrate) configurations. We show that tall nanoparticles exhibit increased scattering cross-sections and support standing wave plasmonic modes, which act to enhance the coupling of light scattered from the nanoparticle into the substrate in a certain wavelength range. Tall nanoparticles are predominantly more forward scattering (in the same direction as the incident light) than backward scattering (in the direction opposite to the incident light). The efficiency with which the light scattered from the nanoparticles is coupled into the substrate depends on the phase shifts introduced at reflection of surface plasmon polaritons at the nanoparticle/air or nanoparticle/Si interface. For particles on the illuminated surface of the cell, the forward scattering nature of these nanoparticles coupled with increased scattering cross-section can lead to efficient light trapping if the coupling efficiency is controlled by varying the phase shifts introduced at nanoparticle/air and nanoparticle/Si interfaces. These results have important implications for designing optimal nanoparticle arrays for light-trapping applications.

We use finite difference time domain (FDTD) numerical modelling using software from Lumerical [17] to study the effect of particle height. Figure 1 shows a schematic of the geometry used for this study. We study a semi-infinite crystalline Si substrate covered with a 20 nm thick SiO_2 layer, typical of surface passivation layers used in solar cells. A silver nanoparticle is placed on top of the oxide. The particles considered in this study are cylinders (diameter 200 nm) with rounded off top and bottom edges (radius of curvature 20 nm). A total field/scattered field (TFSF) source [17, 18], polarized perpendicular to the surface normal (TE polarization) is incident on the particle from the air (or substrate) side, depending on whether we want to simulate nanoparticles on the front (or rear) of the solar cell. A TFSF source is essentially a plane wave source. The nanoparticles behave exactly as they would, if illuminated by a plane wave source. A TFSF source is especially useful for studying the scattering properties of particles, as it allows us to numerically separate the incident field from the scattered field. Similar to the case of a plane wave, where the field in front of the source comprises both incident field and scattered field, but behind the source, all fields measured are due to scattered light; in the case of a TFSF source, we can define a source volume in three dimensions such that fields inside the source volume comprise both incident field and scattered field, while outside the source volume all the fields detected are because of the scattered light (incident field in these regions is subtracted from the total field to numerically give the value of scattered fields). For rear illumination configuration, the source travels 150 nm in the substrate before interacting with the nanoparticles. The monitor positions are indicated with dashed lines. The scattered field monitor is at a depth of 175 nm from the substrate surface. The monitors form five-sided boxes around the nanoparticle in the total or scattered field regions. The sum of power detected across all the monitors in the scattered field region is the total power scattered by the nanoparticle. The ratio of power detected across the monitors in the scattered field region inside Si (monitors represented in green) to the power across all monitors in the scattered field region (in air and in Si) is the fraction of scattered power coupled into the substrate (f_{sub}). The simulation volume (indicated in grey) is defined by perfectly matched layer boundary conditions. We are simulating the case of a single particle and do not account for interactions between adjacent particles. We have shown earlier that single particle simulations provide a good means of predicting the experimental behaviour of random particle arrays [14]. The single particle simulations are likely to give the most accurate representation of experimental results when the surface coverage is $\leqslant 1/Q_{scat}$. In an array of nanoparticles

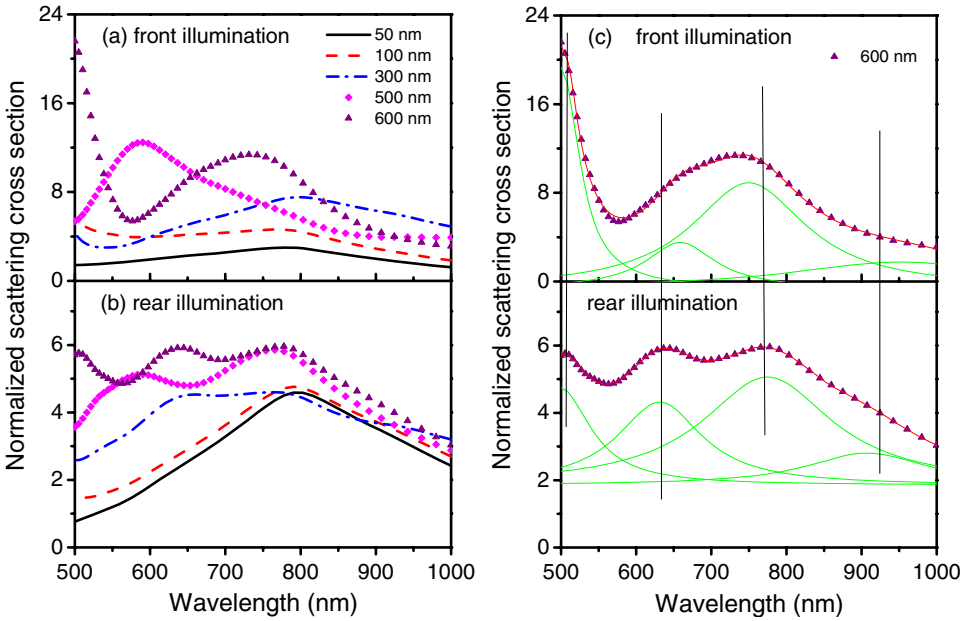

Figure 2. Scattering cross-sections normalized to the cross-sectional area of the nanoparticles as a function of wavelength for nanoparticles on (*a*) the illuminated side (front) of the substrate and (*b*) the rear of the substrate. The nanoparticles are Ag cylinders with a base diameter of 200 nm and varying heights that are indicated in the legend. Note the different vertical scales in (*a*) and (*b*). (*c*) shows Lorentzian fits to the scattering cross-section data for 600 nm tall nanoparticles. The green lines are the Lorentzian components and the red line is the fit to the original data using the Lorentzian components.

with higher surface coverage, the amount of light available for scattering from each particle is reduced, resulting in lower scattering cross-sections. But the major trends observed in the behaviour of the nanoparticles will still be valid.

2. Results and discussion

Firstly, we present results on the scattering cross-section (Q_{scat}) and efficiency with which scattered light is coupled into the substrate (f_{sub}) as the nanoparticle height is varied (section 2.1). We then explain the variations in Q_{scat} and f_{sub} data for tall nanoparticles in terms of standing wave plasmonic modes in section 2.2. In section 2.3, the difference in the behaviour of tall nanoparticles for front and rear illumination configurations is discussed and attributed to asymmetric scattering behaviour of the nanoparticles. Finally, we present results illustrating the effect of Q_{scat}, f_{sub} and asymmetric scattering behaviour of tall nanoparticles on the light-trapping efficiency for both front and rear illumination configurations in section 2.4.

2.1. Scattering cross-section (Q_{scat}) and fraction of scattered light coupled into the substrate (f_{sub})

The scattering cross-section of the metal nanoparticles, Q_{scat} and the fraction of scattered light coupled into the substrate, f_{sub} are important parameters that need to be optimized to maximize the light-trapping efficiency. Figure 2 shows the scattering cross-section, for nanoparticles with varying heights, for both front (*a*) and rear (*b*) illumination configurations. The scattering cross-section is calculated by dividing the power transmitted across all the monitors in the scattered field region (in air and inside the substrate) by the incident power, and normalizing to the cross-sectional area of the nanoparticles. We consider the case of front illumination first. For a particle height of 50 nm or 100 nm, the scattering cross-section peaks at a wavelength of ∼800 nm. The peak magnitude of the scattering cross-section is higher for the 100 nm tall particle, compared to the 50 nm tall particle due to the larger particle volume. The resonance wavelength of the nanoparticles does not shift considerably with increasing particle height because the lateral dimensions of the nanoparticle, which are in the direction of the electric field of the incident source, are fixed. For the same reason, we do not expect quadrupole or higher order charge oscillations in the lateral direction (parallel to the substrate surface) to be excited in the particles, as the particle height is increased. However, we do observe additional peaks in the short wavelength region for taller particles (particle height >100 nm). We attribute these peaks to standing wave resonances of plasmon modes in the taller particles, as described in detail later. It is important to note that as the particle height increases, the magnitude of the peak scattering cross-section of the nanoparticles also increases, which we attribute to the increase in particle volume. On thin waveguides, Q_{scat} would be expected to be further enhanced at wavelengths where each waveguide mode reaches cut-off.

Figure 2(*b*) shows the scattering cross-section for metal nanoparticles on the rear of the substrate. As in the case for nanoparticles on the front of the substrate, the scattering cross-section data for 50 nm and 100 nm tall particles peaks at ∼800 nm. Similar to the data in (*a*), the spectrum broadens with increasing particle height, and additional peaks appear at short wavelengths. When the scattering cross-section spectra

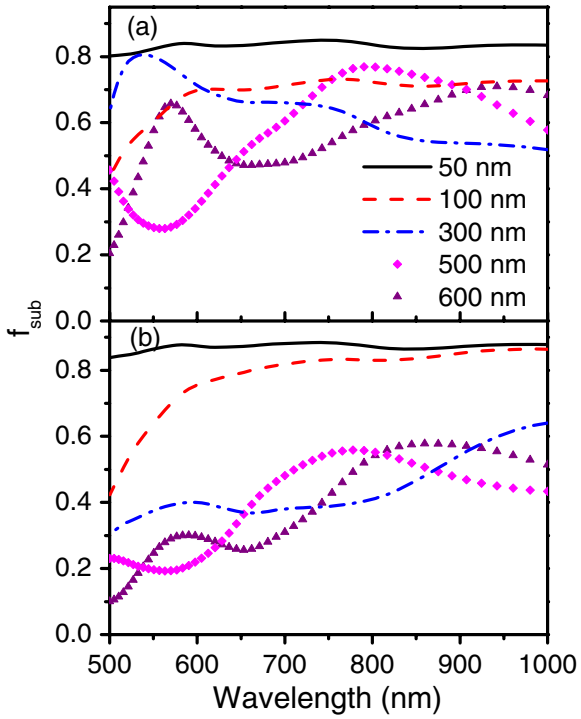

Figure 3. Fraction of scattered light coupled into the substrate (f_{sub}), as a function of wavelength, for varying particle heights for particles (a) on the illuminated surface and (b) on the rear of the substrate. The cross-sectional diameter of the particles is 200 nm. The data are corrected for absorption of scattered light in Si before reaching the monitor.

are deconvolved into Lorentzian peaks, the peak positions for the rear illumination are at the same wavelengths as for the front illumination case. For example, referring to figure 2(c), if we deconvolve the scattering cross-section spectra for a 600 nm tall particle for the front illumination configuration into 3 separate Lorentzians, we find the peaks are at wavelengths of 502 nm, 650 nm, 749 nm and 950 nm, which correspond approximately to the peak positions observed at the wavelengths of 500 nm, 630 nm, 770 nm and 930 nm in the scattering cross-section data for rear illumination configuration.

Figure 2 shows that for particle heights larger than 100 nm the peak scattering cross-section is higher for particles on the illuminated side of the substrate than for particles on the rear of the substrate, for the same particle dimensions. For example, for particles with height 300 nm, the peak scattering cross-section is ∼8 for front illumination and ∼4 for rear illumination. This is due to a difference in the local driving field for the two configurations as studied in detail in [19].

Figure 3 shows the fraction of scattered light coupled into the substrate, f_{sub}, as a function of wavelength, for varying particle heights (indicated in the figure legend), for particles on the illuminated (a) and on the rear (b) surface of the substrate. The data have been corrected for absorption of scattered light in Si before reaching the monitor. For particles on the illuminated surface of the substrate, ∼80% of the scattered light is coupled into the substrate at 1000 nm for a particle height of 50 nm. As the particle height is increased to 100 nm, f_{sub} at 1000 nm is reduced to ∼70%. For particles with height 100 nm f_{sub} is smaller than for particles of height 50 nm for all wavelengths. Increasing the particle height from 50 nm to 100 nm can be understood as moving the effective dipole moment in the nanoparticle away from the substrate surface, reducing the near-field coupling into the substrate [20]. As the particle height is further increased, the spectrum for f_{sub} changes significantly, and local maxima and minima are observed at different wavelengths for different particle heights. For example, for a particle height of 500 nm, we observe a local maximum at ∼780 nm and a local minimum at ∼565 nm. The f_{sub} at the wavelengths corresponding to these local maxima can be higher than the f_{sub} for shorter particles. For example, a larger fraction of scattered light is coupled into the substrate at ∼780 nm for a particle height of 500 nm than for a 100 nm tall particle. It is also interesting to note that at an incident wavelength of ∼600 nm, a pronounced minimum in f_{sub} is observed for 500 nm tall particles, while a maximum is observed for 600 nm tall nanoparticles, a trend opposite to that observed in the cross-section spectra of figure 2.

Similar behaviour is observed for particles on the rear surface of the substrate (figure 3(b)). ∼84% of the scattered light is coupled back into the substrate at 1000 nm for a particle height of 50 nm. As the particle height increases, f_{sub} is reduced. The f_{sub} data exhibit maxima and minima, as in the case of particles on the illuminated surface of the substrate (figure 3(a)). However, for particles on the rear, f_{sub} for tall particles is substantially lower than for particles on the front.

2.2. *Standing wave plasmonic modes*

Figure 4 shows the calculated electric field intensity in the x–z plane, at a wavelength of 500 nm. The particles have a base diameter of 200 nm and a height of 50 nm (a) or 500 nm (b), (c). The positions of the substrate and the dielectric layer are indicated in figure 4(b). The light is incident on the nanoparticles from the substrate side (corresponding to the particles on the rear of a solar cell) for (a) and (b) and from the air side (corresponding to particles on the illuminated surface of the solar cell) for (c). Intensity modulation inside the substrate due to interference of incident and scattered light is clearly visible for the rear-incident configurations in figures 4(a) and (b). For a particle height of 50 nm (figure 4(a)), there is enhanced electric field intensity in the dielectric layer and around the top edges of the particle. These high intensity regions could be a consequence of sharp edges and/or change in the dielectric environment around the particle. For the 500 nm tall particle (figures 4(b) and (c)), in addition to enhanced field intensity at the nanoparticle edges, there is increased field intensity at two positions along the nanoparticle axis, indicated by white arrows. Also, the field intensity around the top edges of the 500 nm tall particle for rear illumination is considerably enhanced compared to the intensity for a 50 nm tall particle.

The high electric field intensity regions along the height of the tall nanoparticles result from interference between up and down propagating surface plasmon polaritons along the nanoparticle surface [21–25]. The wavelength of the surface plasmon polariton propagating inside the nanoparticle (λ_{SPP}) at a given incident wavelength can be determined from the

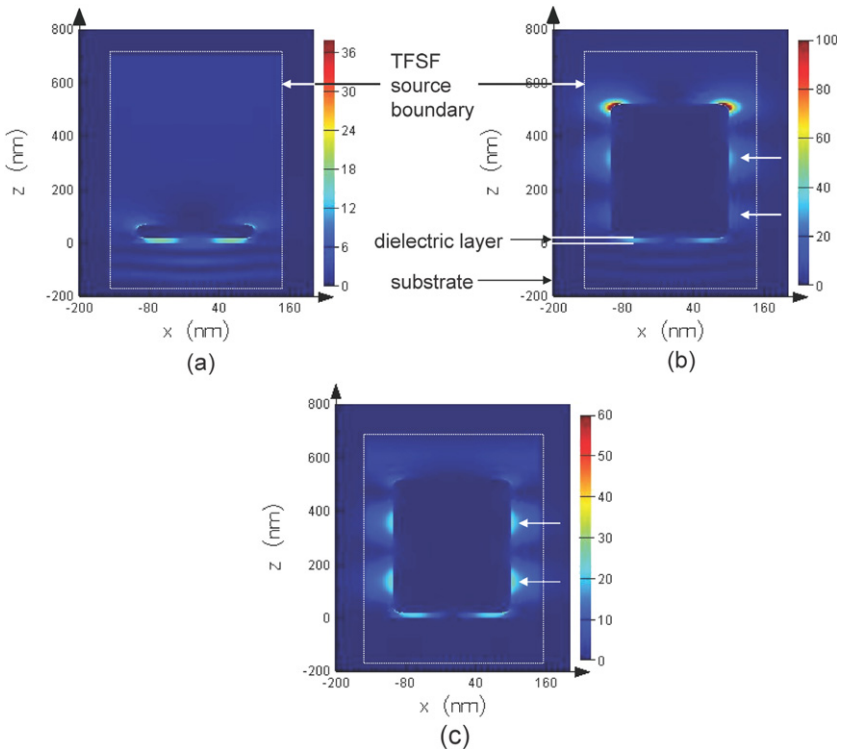

Figure 4. Electric field intensity for incident light at a wavelength of 500 nm, polarized in the x direction in the x–z plane passing through the axis of the nanoparticle. The nanoparticle has a base diameter of 200 nm and a height of (a) 50 nm or (b), (c) 500 nm. The positions of the substrate and the dielectric layer are indicated in (b). The light is incident on the nanoparticles from the substrate side for (a) and (b) and from the air side for (c).

electric field intensity profile at that wavelength. For example from figures 4(b) and (c), λ_{SPP} corresponding to an incident wavelength of 500 nm is ∼420 nm (twice the distance between the regions of high electric field intensity).

The electric field intensity profiles shown in figures 4(b) and (c) can be used to determine the phase shift [21] introduced when the surface plasmon polariton propagating along the tall nanoparticle is reflected back from either the Ag/air interface for the rear illumination configuration or from the Ag/SiO_2 interface for front illumination configuration. Using $\lambda_{SPP} =$ 420 nm and the distance of the electric field intensity maxima from the Ag/air interface for rear illumination configuration, the phase shift introduced due to reflection at Ag/air interface is $\sim 0.3\pi$. Similarly for nanoparticles on the illuminated surface of the solar cell (figure 4(c)), the phase shift introduced due to reflection of the surface plasmon polariton at the Ag/SiO_2 interface is $\sim 0.8\pi$.

The phase shift introduced due to reflection at the Ag/air or Ag/SiO_2 interface, together with the particle height determine the resonance condition for the surface plasmon polaritons in the nanoparticles:

$$2 \times \frac{2\pi}{\lambda_{SPP}} \times h + \Delta\varphi_1 + \Delta\varphi_2 = 2\pi m,$$

where λ_{SPP} is the wavelength of the surface plasmon polariton, h is the nanoparticle height, $\Delta\varphi_1$ and $\Delta\varphi_2$ are the phase differences introduced due to reflection at the Ag/air and Ag/Si interface, respectively, and m is an integer. For λ_{SPP} satisfying above condition, the nanoparticles resonantly scatter the incident light, resulting in the peaks at short wavelengths in the scattering cross-section data, as seen in figures 2(a) and (b).

We now explain the coupling efficiency (f_{sub}) data shown in figure 3. As already mentioned, the peaks in f_{sub} for tall nanoparticles correspond to the minima (off resonance) in scattering cross-section data shown in figure 2 and the minima in f_{sub} correspond to maxima (resonance) in the scattering cross-section. The efficiency with which light scattered by the nanoparticles is coupled to the substrate depends on the field intensity distribution along the nanoparticle. Higher field intensities close to Ag/Si interface enhance near-field coupling of scattered radiation, resulting in a larger fraction of scattered light being coupled into the substrate. Figure 5 shows the ratio of the intensity at the far end to the intensity at the near end of the nanoparticle as a function of the phase shift introduced at reflection from the near end and the far end. The data in figure 5 have been obtained using the analytical expressions for electric field intensity along a one-dimensional resonator, given in [21]. In the model, the wave vector is varied so that the resonator is either exactly on resonance (figure 5(a)) or off resonance (figure 5(b)). For front illumination configuration, the near end is the Ag/air interface and the far end is the Ag/Si interface (inset of figure 5). For this configuration, larger field intensity at the far end of the nanoparticle results in better coupling efficiency. As already described, the phase shift at $\lambda_{SPP} = 420$ nm is 0.3π at the near end and 0.8π at the far end. The region marked by white circles in figure 5 corresponds to these phase shifts. When the nanoparticle is on resonance (figure 5(a)), the field intensity at the far end of the nanoparticle

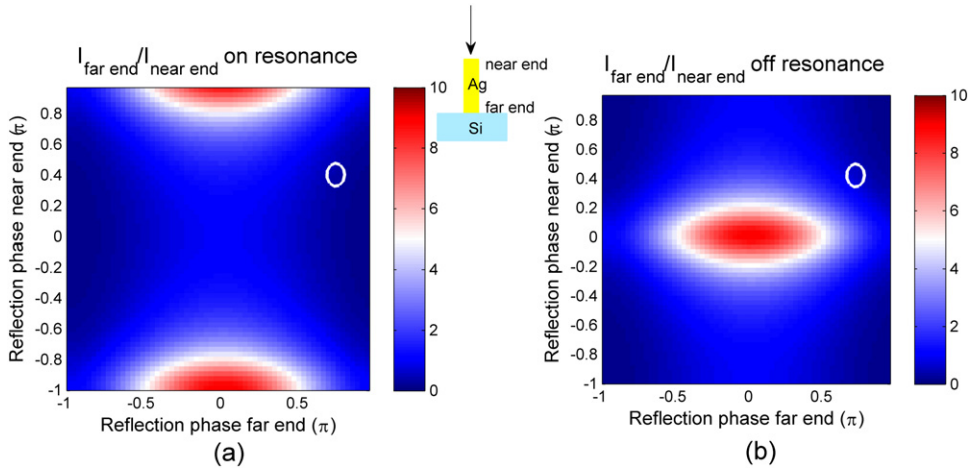

Figure 5. Ratio of far-end intensity to near-end intensity, as a function of phase shift introduced at reflection at the far end and near end of a nanoparticle when the nanoparticle is (*a*) on resonance ($m = 1$) and (*b*) exactly off resonance ($m = 1/2$). The region marked by white circles corresponds to the phase shifts introduced at reflection for front illumination configuration. The inset illustrates the far end and near end for front illumination configuration.

(Ag/Si interface) is only a fraction of the field intensity at the near end of the nanoparticle (Ag/air interface), resulting in poor coupling efficiency. When the nanoparticle is off resonance (figure 5(*b*)), the field intensity at Ag/Si interface is much larger than the field intensity at Ag/air interface, leading to better coupling efficiency.

The coupling efficiency of the nanoparticles depends critically on the phase shifts introduced at reflection from the Ag/air and Ag/Si interfaces. From figure 5, we can infer that a far end (Ag/Si interface) phase shift close to zero will result in better coupling efficiency for any phase shift introduced at the near end (Ag/air interface), both on resonance and off resonance. However, a near-end phase shift of $\pm\pi$ is ideal for maximal coupling efficiency when the nanoparticle is on resonance.

2.3. Difference in nanoparticle behaviour for front and rear illumination configurations

The results presented so far indicate that tall nanoparticles have a larger scattering cross-section and the fraction of scattered light coupled into the substrate is locally enhanced or reduced because of excitation of standing wave plasmonic modes. Now we proceed to study the differences in nanoparticle behaviour for front and rear illumination configurations. For a nanoparticle height of 50 nm, the fraction of scattered light coupled into the substrate is similar for both front (figure 3(*a*)) and rear (figure 3(*b*)) illumination configurations. For 100 nm tall particles, a slightly larger fraction of light is coupled into the substrate when the nanoparticles are located on the rear surface of the substrate compared to the case where the nanoparticles are placed on the illuminated surface of the cell. But for taller particles ($h \geqslant 300$ nm), f_{sub} is substantially higher when nanoparticles are on the illuminated surface of the substrate than when the particles are on the rear of the substrate. This behaviour can be explained in terms of asymmetry between forward (in the same direction of incident light) and backward (in the direction opposite to the incident light) scattering from the nanoparticles, as the nanoparticle height is varied, as discussed below.

Figure 6 shows the far-field angular distribution of the intensity of the scattered radiation with wavelength 1000 nm from nanoparticles in air (i.e. without a substrate) in the *xz* and *yz* planes, as the nanoparticle height is varied. The data are obtained using the set-up shown in figure 1 by removing the Si substrate. A far-field transformation is applied to the data recorded by the monitors shown in figure 1. The far-field transformation requires a uniform dielectric environment around the nanoparticles, and thus cannot be used if the nanoparticles are on a substrate. An angle of 0° corresponds to forward scattering while 180° corresponds to backward scattering. For a nanoparticle height of 50 nm, the angular distribution of scattered radiation closely resembles that of a point dipole and the forward and backward scattered light intensity distributions are comparable (figure 6(*a*)). This explains the almost equal values for f_{sub} for front and rear illumination configurations (figures 3(*a*) and (*b*)), for a nanoparticle height of 50 nm. As the nanoparticle height is increased to 100 nm or 300 nm, the particles scatter more radiation in the backward direction than in the forward direction (figures 6(*b*) and (*c*)). For example, back scattered light (integrated over all angles) is 1.3 times as intense as forward scattered light for particle height of 100 nm. The more back scattering nature of these nanoparticles corresponds to an increased f_{sub} at 1000 nm when particles with height $\leqslant$300 nm are placed on the rear surface of the substrate compared to the case where the particles are placed on the illuminated surface of the substrate.

As the nanoparticle height is further increased, the far-field angular distribution pattern changes from more back-scattering to more forward scattering (as illustrated in figure 6(*d*)). For example, forward scattered light is 4 times as intense as back scattered light for particle height of 500 nm. The more forward scattering nature of tall nanoparticles corresponds to the increased f_{sub} observed in figure 3 when particles with height >300 nm are placed on the illuminated surface of the

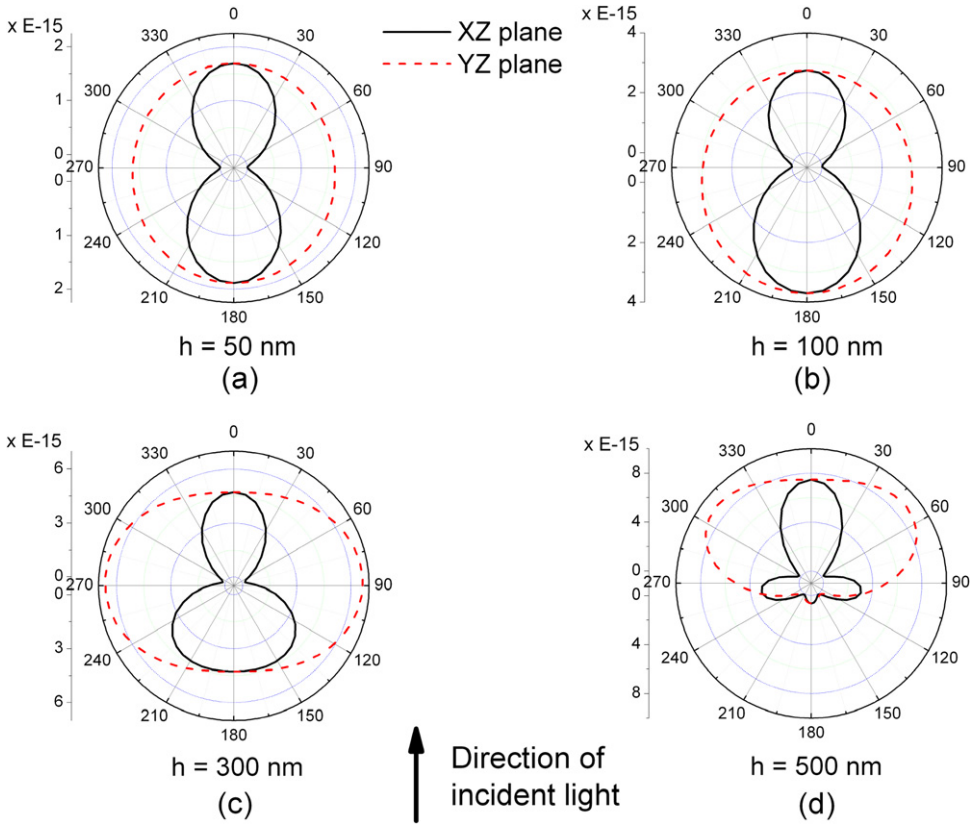

Figure 6. Far-field angular distribution of scattered radiation (wavelength 1000 nm) in *xz* and *yz* planes for incident light polarization in *x* direction. The Ag cylinders simulated are in air (no substrate), have a base diameter of 200 nm and a height of 50 nm (*a*), 100 nm (*b*), 300 nm (*c*) or 500 nm (*d*).

substrate compared to the case where the particles are placed on the rear of the substrate.

The forward–backward asymmetry in the angular distribution of scattered radiation from the nanoparticles is a consequence of increasing particle size. Our results are similar to the asymmetry observed in angular distribution of scattered radiation from homogeneous spheres with increasing size [26]. As already mentioned above, the data shown in figure 6 are for nanoparticles in air (not on a substrate). The presence of a substrate will change the angular distribution of scattered radiation; however, these data provide a qualitative explanation for the difference in the trends in f_{sub} with particle height for particles on the front and rear surface.

2.4. Effect of Q_{scat}, f_{sub} and asymmetric scattering behaviour of nanoparticles on light-trapping efficiency

The power scattered into the substrate from the metal nanoparticles depends on the magnitude of the scattering cross-section and the fraction of scattered light coupled into the substrate (f_{sub}). For particles on the illuminated surface of the substrate, a large increase in the magnitude of scattering cross-section is observed (figure 2(*a*)) accompanied by a slight decrease in f_{sub} (figure 3(*a*)), as the nanoparticle height is increased. For example, at a wavelength of 1000 nm, the scattering cross-section is increased from 1.3 to 3.0 and f_{sub} is reduced from 0.80 to 0.66 as the nanoparticle height increases from 50 to 600 nm. These numbers would mean that 2 times more light at 1000 nm would be scattered by a 600 nm tall nanoparticle compared to a 50 nm tall particle. However, only 66% of the scattered light is coupled into the substrate with a 600 nm tall nanoparticle while 80% of the scattered light is coupled into the substrate with a 50 nm tall nanoparticle. If the phase shift introduced at reflection from the Ag/Si or Ag/air interface can be engineered to increase f_{sub}, the increased scattering cross-section of tall nanoparticles on the illuminated surface of the solar cell could be used for efficient light trapping. For example, the phase shift introduced at the Ag/air interface can be increased by coating the nanoparticle surface with a higher refractive index material.

Figure 7 shows the fraction of scattered light coupled into the substrate (f_{sub}) for a 500 nm tall nanoparticle, with or without a Si coating on the top. The bottom panel shows the Q_{scat} data for the nanoparticle along with the Lorentzian fits. The vertical black lines match the peaks at resonance in Q_{scat} data to dips in f_{sub} data for a bare nanoparticle. As can be seen from the figure, the f_{sub} at the Q_{scat} resonance peaks can be increased by coating the nanoparticle surface with Si, which modifies the phase shift introduced at reflection into the surface plasmons. The phase shift introduced at the nanoparticle interface is increased to $\sim 0.6\pi$ by coating the interface with Si.

For the values of f_{sub} estimated in this study, the expected path length enhancement that can be achieved by using tall nanoparticles can be estimated assuming that the nanoparticles scatter all the light incident on them [11], which is a reasonable

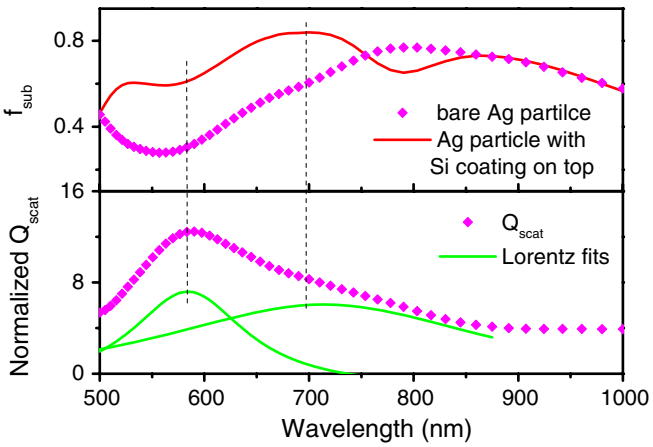

Figure 7. Fraction of scattered light coupled into the substrate (f_{sub}) as a function of wavelength, for a 500 nm tall bare Ag nanoparticle and a Ag nanoparticle with top surface coated with Si, placed on the front of the solar cell. The bottom panel shows the Q_{scat} data and the Lorentzian fits for the 500 nm tall nanoparticle.

assumption given the high scattering cross-sections estimated for tall nanoparticles (figure 2). The average path length enhancement is given by the expression $2d_{average}/(1 - f_{sub})$, where $d_{average}$ is the ratio of average path travelled by the scattered light in a single pass through the solar cell to the cell thickness. We calculate $d_{average}$ numerically using Lumerical (details of the calculation will be published elsewhere) and use the f_{sub} values shown in figure 3. Using nanoparticles with height 500 nm on the illuminated surface of the solar cell can provide path length enhancements of ∼6, ∼11 and ∼10 at incident wavelengths of 700 nm, 800 nm and 900 nm, respectively. By increasing the f_{sub} by coating the nanoparticle surface with Si (as shown in figure 7), the path length enhancement at incident wavelength of 700 nm is increased to ∼16.

For particles on the rear of the substrate, a small increase in the magnitude of the scattering cross-section (figure 2(*b*)) accompanied with a large reduction in f_{sub} (figure 3(*b*)) is observed. For example, at a wavelength of 1000 nm, the scattering cross-section is increased from 2.4 to 3 and f_{sub} is reduced from 0.84 to 0.49. So, as the particle height increases from 50 nm to 600 nm, the amount of light scattered into the substrate would decrease by a factor of 0.73. The modest increase in scattering cross-section coupled with a large reduction in f_{sub} results in less light scattered into the substrate for taller nanoparticles on the rear of the substrate.

3. Conclusions

We have systematically studied the scattering, near-field coupling and plasmon standing waves in tall Ag nanoparticles on a Si substrate. We have shown that by increasing the nanoparticle height, its scattering cross-section is increased. However, the efficiency with which scattered light is coupled into the substrate is reduced for taller nanoparticles due to an increase in effective distance between the effective dipole moment and the substrate. Varying particle height also changes the forward/backward scattering ratio, and thereby the near-field coupling.

For front illumination configuration, a large increase in scattering cross-section is observed in conjunction with a slight reduction in coupling efficiency (f_{sub}). The increase in scattering cross-section for tall nanoparticles could be employed for efficient light trapping by modifying f_{sub} by engineering the phase shift introduced at reflection from Ag/Si interface or Ag/air interface.

The f_{sub} values estimated in this work show that for front illumination configuration, path length enhancement of ∼11 and ∼10 can be achieved at illumination wavelengths of 800 nm and 900 nm, respectively, when 500 nm tall nanoparticles are used. The estimated path length enhancement at 700 nm for a 500 nm tall nanoparticle coated with Si is ∼16. We have thus shown that tall nanoparticles on the illuminated surface of the solar cell act as nano-antennas, effectively channelling incident radiation into the substrate at large angles, thereby increasing the path length and hence absorption in the solar cell.

For particles on the rear of the substrate a modest increase in scattering cross-section and a large reduction in coupling efficiency is observed, making tall particles less efficient than short nanoparticles for light trapping applications.

Acknowledgments

The authors thank the Australian Research Council for financial support. SARA, Amsterdam, is thanked for computing services. The Dutch part of the work is part of the research program at FOM which is financially supported by NWO and the Joint Solar Program.

References

[1] Derkacs D, Lim S H, Matheu P, Mar W and Yu E T 2006 *Appl. Phys. Lett.* **89** 093103
[2] Catchpole K R and Pillai S 2006 *J. Appl. Phys.* **100** 044504
[3] Pillai S, Catchpole K R, Trupke T and Green M A 2007 *J. Appl. Phys.* **101** 093105
[4] Keisuke N, Katsuaki T and Harry A A 2008 *Appl. Phys. Lett.* **93** 121904
[5] Catchpole K R and Polman A 2008 *Opt. Express* **16** 21793–800
[6] Polman A 2002 *Nature Mater.* **1** 10–12
[7] Atwater H A and Polman A 2010 *Nature Mater.* **9** 205–13
[8] Schaadt D M, Feng B and Yu E T 2005 *Appl. Phys. Lett.* **86** 063106
[9] Matheu P, Lim S H, Derkacs D, McPheeters C and Yu E T 2008 *Appl. Phys. Lett.* **93** 113108
[10] Derkacs D, Chen W V, Matheu P M, Lim S H, Yu P K L and Yu E T 2008 *Appl. Phys. Lett.* **93** 091107
[11] Catchpole K R and Polman A 2008 *Appl. Phys. Lett.* **93** 191113
[12] Xu G, Tazawa M, Jin P, Nakao S and Yoshimura K 2003 *Appl. Phys. Lett.* **82** 3811–3
[13] Mertens H, Verhoeven J, Polman A and Tichelaar F D 2004 *Appl. Phys. Lett.* **85** 1317–9
[14] Beck F J, Polman A and Catchpole K R 2009 *J. Appl. Phys.* **105** 114310
[15] Akimov Y A, Koh W S and Ostrikov K 2009 *Opt. Express* **17** 10195–205

[16] Mokkapati S, Beck F J, Polman A and Catchpole K R 2009 *Appl. Phys. Lett.* **95** 053115
[17] *Lumerical FDTD Solutions* (www.lumerical.com)
[18] Taflove A and Hagness S C 2005 *Computational Electrodynamics The Finite-Difference Time-Domain Method* 3rd edn (Boston, MA: Artech House Publishers)
[19] Beck F J, Mokkapati S, Polman A and Catchpole K R 2010 *Appl. Phys. Lett.* **96** 033113
[20] Soller B J, Stuart H R and Hall D G 2001 *Opt. Lett.* **26** 1421–3
[21] de Waele R, Burgos S P, Polman A and Atwater H A 2009 *Nano Lett.* **9** 2832–7
[22] Schider G, Krenn J R, Hohenau A, Ditlbacher H, Leitner A, Aussenegg F R, Schaich W L, Puscasu I, Monacelli B and Boreman G 2003 *Phys. Rev.* B **68** 155427
[23] Vesseur E J R, de Waele R, Kuttge M and Polman A 2007 *Nano Lett.* **7** 2843–6
[24] Dorfmüller J, Vogelgesang R, Weitz R T, Rockstuhl C, Etrich C, Pertsch T, Lederer F and Kern K 2009 *Nano Lett.* **9** 2372–7
[25] Novotny L 2007 *Phys. Rev. Lett.* **98** 266802
[26] Bohren C F and Huffman D R 2004 *Absorption and Scattering of Lght by Small Particles* (Weinheim: Wiley-VHC)